Exploration of Hypomyelination in Extreme Preterm Infants through n-Compartment Models

Rudy C. Yuen
20000153

Abstract

Extreme Preterm Infants (EPTs) are known to have a decreased amount of myelin in their white matter regions compared to non-EPTs, which leads to complications with neurological growth during adolescence. It prompts an active research into their intercerebral structure through the use of T2 Magnetic Resonance Imaging (MRI).

T2-weighted MRIs are captured by measuring the amplitude of echoes generated using specific echo techniques at fixed time intervals after the deactivation of a Radio-Frequency (RF) Magnetic Field. The relationship between the amplitude of these echo signals and the time after the RF pulse is deactivated is known to exhibit an exponential decay. In regions containing more than one tissue type, it has been seen to be more accurate to employ a multiple-compartment exponential decay model due to the fact that this approach takes into account the complex tissue compositions by assuming each tissue type contributes its own characteristic decay rate.

As EPTs have a decreased amount of myelin in their brain, we hypothesise that the average compartments needed voxel-wise to model the white matter is lesser for an EPT than a non-EPT. This is because an EPT has fewer myelins within the white matter of their brain, meaning that there are lesser tissue types per voxel. We provided a counter-evidence towards this hypothesis through a simpler version of the experiments due to computational constraints. This counter-evidence has been shown using a one-tailed student's T-Test.

1. Introduction

Extreme Preterm Infants (EPT) refer to births before 26 weeks of gestation. EPTs have been seen to be more likely to exhibit different neurological growth and exhibit developmental disabilities in the first two years of life [1].

This difference has been shown to be due to a decreased amount of myelin in EPT's brains as opposed to a non-EPT infant. Since myelin has been shown to be responsible for cognition, learning, skill development and memory [2], the lack of myelin can impact an EPT's growth, causing a decrease in the EPT's intellectual capability. It has been shown that 41% of EPTs have experienced cognitive impairment, where this impairment is defined by having a test score that is 2 standard deviations below the mean of their peers at 6 years of age [1].

This demonstrates the importance of identifying areas that an EPT would need support on. EPICure has been instantiated to study MRI sampled from EPT infants [3]. Throughout the course of the study from 1995, EPTs who were born between 22 to 26 weeks of gestation have been studied. Follow up on these EPTs have been done at 1, 2.5, 6, 11, 16 and 19 years old to extensively measure their physiological and psychological growth, where an MRI is taken at 19 years of age for each EPT.

In order to better assist EPTs during adolescence physiologically and through their learning journey, it is paramount to understand the differences in their brain and a non-EPT to identify regions that are severely unmyelinated. This can be done by analysing the Magnetic Resonance Images (MRI) of the EPT, where we can identify regions inside their brain which is less developed. For example, using EPICure's data, it has been shown that multiple brain regions such as the Corpus Callosum is less myelinated in EPTs through the use of a 2-compartment model which will be introduced in section 1.2 [4]. It has also been shown that hypomyelination in the splenium of the corpus callosum can lead to structural and psychological alterations which are still visible throughout adolescence [4].

1.1. T2 Relaxometry

Magnetic Resonance Images (MRI) are generated by capturing the intrinsic magnetic properties of intracerebral tissues [5]. When an MRI is taken, a strong primary magnetic field B_0 is applied to the brain, which aligns

the nuclear spins of the hydrogen atoms within the water molecules inside the brain. This alignment is made to be parallel to the direction of the applied magnetic field. A radio-frequency (RF) pulse perpendicular to the magnetic field is then applied in the orthogonal direction to B_0, exciting the protons and flipping them out of their initial state to a higher energy state.

As the RF pulse is deactivated, the protons relax therefore emitting an RF signal which is then detected by the MRI machine. The T1, T2 and T2* values can be estimated using the appropriate pulse sequence and parameters. The map of these values estimated from protons relaxing is referred to as relaxometry [6].

T2-weighted MRI is captured by measuring the amplitudes of echoes generated using specific echo techniques at fixed time intervals after the deactivation of the RF magnetic field. These fixed time intervals are also known as echo times TE.

T2 relaxometry has been found to be useful for quantifying signal changes on T2-weighted MRI, which is more useful for myelin detection than T1 relaxometry as T2 relaxation times are more sensitive to the presence of myelin in neural tissues. This helps radiologists to understand the distribution of myelin in the brain, for example demyelinating diseases would give a bright area on the T2 image as the regions which should contain myelin has now got an increased water content. A similar concept applies for EPTs.

Other than understanding myelin, T2 relaxometry can also help radiologists in understanding the human anatomy. This is since T2 relaxation rate are different in different parts of body, creating contrast within the MRI image, enabling radiologists to detect irregularities, such as cerebral edema and cancer, therefore providing proper diagnosis to a patient.

The de-phasing of these spins are known to exhibit an exponential decay, where it can be modelled naively as $S_{TE} = S_0 \exp(-\frac{TE}{T2})$. Parameters within this model can be estimated using the linear regression's normal equation after taking logs if we ignore the distribution of the noise within each measurements. This is, we model the expression as: $\log(S_{TE}) = -\frac{TE}{T2} + \log(S_0)$ and subsequently use the normal equation if we define the ith row of design matrix X to be $\begin{bmatrix}1 & TE_i\end{bmatrix}$ and $y_i = \log(S_{TE_i})$, then solve the expression below:

$$\begin{bmatrix}-T2^{-1} \\ \log(S_0)\end{bmatrix} = (X^T X)^{-1} X^T y$$

The verification of this exponential decay relationship instead of a linear decrease relationship can be seen in Figure A.3. Each pixel in this map measures $1 - r^2$ where r^2 is the coefficient of determination, measuring how much the voxel in that slice follows a linear decrease and exponential decay against echo time.

We create a map of $1 - r^2$ to better visualise the regions that most violates the hypothesised relationship in Figure A.3. In this particular slice, we can see that the cerebrospinal fluid (CSF) region hosts the brightest pixels, demonstrating that the signal intensity against the echo time in the CSF follows neither a linear decrease nor exponential decay. This is because T2 times in CSF regions are significantly longer than the longest echo time, causing it to be difficult to fit an exponential decay to it, where Pareto and super-hyper exponential models could be a better fit.

However, in general, we observe that the exponential decay map is much dimmer than the linear decrease map, which demonstrates the underlying relationship between signal intensity and echo times follows a exponential decay more than a linear decrease.

We have also visualised the signal intensity against the echo time for white matter segmentation-wise average. We can see that after taking logs on both sides the curve looks more linear than without taking logs on both sides in Figure A.4, further suggesting that the relationship between signal intensity and echo time is an exponential decay.

Although this estimation using the normal equation, which we will hereby refer to as the 'exponential decay', gives only a rough estimate of the output as we ignore the noise distribution, the estimated parameters can be served as a starting point to fit the one-compartment model, which has the exact same model function as the exponential decay, but is fitted through gradient descent on the sum of squared errors, if we assume the noise distribution is Gaussian. We can also use the Rician loss, which has been seen to be a more accurate estimation of MRI noise than Gaussian [7] if the observation's noise is previously known quantitatively. Rician loss is modelled by the following, with σ being the observation's noise parameter.

$$L_{\text{Rician}}(x; y) = -\sum \left(log(y) - \frac{x^2 + y^2}{2\sigma^2} + \log\left(I_0\left(\frac{xy}{\sigma^2}\right)\right)\right)$$

We can see that the difference between the generated map for S_0 and T_2 from the exponential decay model (Figure A.1) and one-compartment model (Figure A.2) are very subtle in the white matter region. However, regardless of the minimal difference, we can see that Figure A.2 is brighter than Figure A.1, and the scale for Figure A.2

is also smaller than A.1. This demonstrates that the noise in Figure A.2 is weaker than Figure A.1. This highlights the importance of taking into account of the noise distribution, which can only be done through performing a gradient descent with a loss function that represents the true relationship of the noise distribution.

1.2. Multiple Compartment Models

Due to technological restrictions where MR imaging cannot captured at a cellular resolution, it might occasionally be true that there are more than one tissue types captured within one voxel of the MRI.

Since different tissues within the brain are known to have different water content implying different hydrogen atom concentrations and direction of flow, it has been shown to be more accurate to use a multi-compartment model to model one voxel within the brain, encapsulating the fact that there are potentially more than one tissue type within one voxel [8].

The n-compartment model is modelled as equation 1. In this expression, we introduced different T2 times, denoted as $T2_i$ with its corresponding volume fraction υ_i. The volume fraction indicates the proportion of the voxel being that particular tissue:

$$S_{TE} = S_0 \sum_i^n \upsilon_i \exp\left(-\frac{TE}{T2_i}\right) \tag{1}$$

Since the volume fraction must add to 1, we can denote the last volume fraction $\upsilon_n = 1 - \sum_i^{n-1} \upsilon_i$. Therefore, there are $2n$ parameters to fit in this model.

Minimisation over this expression should take into consideration that this model is prone to overfit if we use too much compartments. Furthermore, to avoid overfitting by overdetermination, it is imperative that the number of parameters in model we fit does not exceed the number of observations we have.

To ensure that the model's parameters are physiologically sensible, we assert positivity with $T2_i$ and S_0 by fitting its squared value instead. We also take a sigmoid to ensure that $0 \leq \upsilon_i \leq 1$. The constraint $1 \geq \sum_i^{n-1} \upsilon_i \geq 0$ is imposed, as it is not sensible for the volume fractions to add up to a value that is not 1.

We can see in Figure A.5 that the 2-Compartment Model fits better than the Exponential Decay model when we focus on the head of the graphs. To evaluate the necessity of increase a compartment into the model, we can use the Akaike Information Criterion (AIC). The AIC aims to provide an estimate for the model that will be closest to the true model in terms of the Kullbeck-Leibler information criterion. The AIC can be used for model selection, where the model with the best fit will have the lowest AIC.

Model	AIC (3 s.f.)
Exponential Decay	99.02
1-Compartment Model	87.30
2-Compartment Model	62.90

Table 1: AIC for different fittings

AIC for sum of squared loss is modelled by $AIC = 2k - K\log(K^-1l)$, where l is the sum of squares loss, amount of observations K and k being the amount of parameters to fit.

The AIC of the 3 models in Figure A.5 are illustrated in Table 1. We can see that the AIC is significantly lower in the 2-Compartment Model than the 1-Compartment Model in the White Matter region. Note that the compartment models takes in initial parameters fitted through the normal equation and tunes it accordingly.

It is also worth noting that the exponential decay model has a higher AIC than the 1-compartment model, further highlighting the importance of respecting the noise distribution of the data.

2. Methods

Figure A.6 is a cross section of the white matter under an electron-microscope. It can be seen that there are many other tissue types other than the myelin in this image, such as intra-axonal regions, extra-cellular regions and free water content. Electro-microscopes are not used to capture a patient's MRI as it requires to slice the brain's cross section. As a tradeoff, MRIs are unable to operate at the same resolution as electro-microscope, and cannot reach cellular resolutions. This means that signals from multiple types of tissues are obscured within one voxel's echo time against signal intensity graph.

This demonstrates the necessity to use multiple compartment models to model the signal intensity against the echo time to obtain the T2-times and volume fractions of each tissue type. This allows us to uncover the obscured signals and subsequently analyse the volume fractions of different tissues in the brain provided that we know the range of T2 times we are expecting from the tissue that we are interested in analysing.

To discover the necessity of the usage of a multi-compartment model, we use a dataset composed of T2-MRI that is taken with 21 echo times, which we refer to as the 'HD Dataset'. We sample one patient from the HD

Compartments	Voxels
1	370
2	606
3, 4, 5	0

Table 2: Count of Voxels having lowest AIC in the n-Compartment Model

Dataset, where we take a slice from his brain's white matter in the axial view to compute the best amount of compartments to model each voxel to create Figure A.7.

To determine the best amount of compartments, we vary the compartments from 1 to 5, where we determine the best amount of compartments by a best trade-off between number of parameters and the sum of squared loss. This trade-off is measured using the Akaike Information Criterion (AIC), where the best model will have the smallest AIC. We also create a map of the AIC for each voxels for each compartment model we used in Figure A.8.

Whilst the difference between different compartment models' AICs are rather minimal when we look at Figure A.8's color bars, Figure A.7 suggests that there are more voxels in the slice that we chose that would best fit towards a 2-compartment model in this dataset. There are a total of 976 voxels in this slice, where the amount of voxels best fitting towards each amount of compartment is as the table 2.

2.1. Dataset

Whilst the HD Dataset consists of more echo times, it is not labelled whether a patient is an EPT or not, and we do not have a large population of data as well. Hence, we will use EPICure's data instead of the HD Dataset for this study.

The EPICure dataset consists of MR images of 89 EPT and 54 non-EPTs at the gender split of 52/37 and 32/22 F/M respectively[1]. Other than their T2-weighted MRI, the dataset consists of information such as all subject's gestation age at birth (GAB), intelligence quotient and sex.

All MRIs used in this study are captured when the subject is 19 years old. All T2 MRIs consists of 10 echo times, where this implies that we cannot fit more than 5 compartments into the model to avoid overdetermination.

2.2. Experimental Hypothesis

Since we know that EPTs have a lesser amount of myelin, this increase the chances that the signal coming from the myelin is obscured by the signal produced by other tissue types where this obscurity cannot be uncovered by the use of a multi-compartment model. Hence, we hypothesise that the amount of compartments needed to optimally model the white matter regions in EPT's brains are lesser than what is needed for non-EPTs.

To demonstrate this solidly, it is imperative to check every single voxel in the EPICure dataset, in that we compute the amount compartments that best fits each voxel. Using this series of numbers for all the voxels, we compute the average amount of compartment to optimally fit the white matter for each patient. We will then have two lists, a list of average amount of optimal compartments for EPTs and another for non-EPTs which we can use to perform a T-test.

However, due to time and computational constraints, we are unable to compute this. Yet, we provide the code which execute this as part of Future Works[2]. We will also discuss this further in depth in Section 4.3.

Taking a trade-off between computational constraints and experimental outcome, we take the average for all white matter voxels to obtain an estimation of the best amount of compartments that best fit this patient's white matter voxels. This can increase the Signal to Noise Ratio as averaging can remove the noise within sampling. Although this approach is sub-optimal in answering our initial research question, it provides an insight into the validity of our approach.

After executing the code, we will have an integer indicating the best amount of compartments for each patient's white matter segmentation average. We then perform a Student's T-Test to see whether if it is significant enough to say that non-EPT's brains require more compartments to model.

The null hypothesis of our study is that the amount of optimal compartments for EPTs and non-EPTs are the same, and the alternate hypothesis is the amount of optimal compartments for EPTs is smaller than non-EPTs. This would require a one-tailed T test, where we use a significance level of 5%.

2.3. Fitting Technique

Python 3.11 will be used in this study; a detailed list of packages used in the virtual environment for this study has been provided as a requirements text file. In particular, we perform constrained minimisation using `scipy.optimize.minimize`.

[1] This does not match Professor Melbourne's PowerPoint. I did not seek for why as missing one or two patients' data does not impact the results of this experiment significantly.

[2] See code `epicure-runscript.py` in submission

Mathematically, for any amount of compartments n, we aim to minimize the equation 2, where $f(\cdot)$ denotes the n-Compartment model, modelled as equation 1.

$$\underset{\upsilon_i, S_0, T2_i}{\arg\min} \sum_i (S_{TE_i} - f(TE_i))^2 \tag{2}$$

To reduce the difficulty of the fitting problem, we remove υ_n from the parameters that is to be fitted. Instead, we define $\upsilon_n = 1 - \sum_i^{n-1} \upsilon_i$. Therefore the constraint of this fitting problem becomes $1 \geq \sum_i^{n-1} \upsilon_i \geq 0$.

To create a starting x to fit the multiple compartment model, we use parameter priors from the exponential decay model. We define S_0 in the multiple-compartment model to be the same as what we found in the exponential decay normal equation. We also define $T2_i = \frac{T2_{ne}}{i}$ where $T2_i$ is the $T2$ time for compartment i and $T2_{ne}$ as the T2 time found in the normal equation. This would effectively create a list of long and short T2 times.

The starting volume fraction will be the same for all compartments, where it equals to $\frac{1}{n}$. We avoid being trapped in a local minima due to a poor initialisation value by permuting the starting x using the permutation size modelled as below.

$$5 \times 10^{\lfloor \log_{10}(x_0^{(i)}) \rfloor}$$

We permute the starting x for 100 times and complete the minimisation on each of the starting xs. For the 100 minimisation instances, we take the best instance, which is defined by the smallest loss. We then compute the AIC for that instance.

To ensure that the fitted x is within range, we perform a transformation. We expect S_0 and T2 Time T_2 to be positive, which can be asserted by taking a square, and $0 < \upsilon_i < 1$, which can be enforced using a sigmoid.

2.4. Segmentation Mask

During an MRI, it is unavoidable that the patient's head moves during the study, which causes a misalignment to each MRI taken. To readjust each slice on the MRI back together, Geodesic Information Flows are used to negate the effect of head movement. This algorithm is also able to provide a label to the segmentation on each voxel, which indicates the segmentation that the voxel belongs to [9].

EPICure used Geodesic Information Flows to remove the effect of head movement. Since each label computed by Geodesic Information Flows is not binary, we will require a threshold value which we take any value above the threshold value as the mask for the segmentation. Upon trial and error, we discovered that the mask $\sigma^{-1}(0.6)$ seemed to be viable to capture all white matters. Note that σ^{-1} is the inverse sigmoid. A sample of the mask computed this way has been placed as Figure A.9.

Patient ID	EPT	M/F	GAB
43607	False	F	40
44631	True	M	25
74067	True	M	25
78004	True	M	25

Table 3: Poor Data

2.5. Data Cleaning & Excluded Data

We clean our data by removing patient's T2 MRI that does not satisfy either of the two requirements: 1. the file is corrupted, and/or 2. there are lesser, or more than 10 echo times taken with the MRI. Patient ID 43607's quantified T2 map is corrupted[3], whereas patients with IDs 44631, 74067 and 78004 have insufficient amount of echo times with their MRI, where they have 8, 2 and 7 echo times respectively.

Information regarding the 4 patients that are removed from the study have been provided in Table 3.

3. Results

Taking on the data sampled, we perform several student's T-test to find whether multiple compartment models can be used as an indicator to distinguish EPT and non-EPT's T2 MRI.

3.1. Difference between Optimal Compartments

Our first analysis is to compare the average of the best amount of compartments for each patient white matter segmentation average. The EPTs required an average of 1.116 compartments to model their white matter regions; whilst non-EPTs required an average of 1.208 compartments. To distinguish whether there is a difference, we perform a one tailed T-test, where the p-value for the one-tailed T-test is half the p-value for the two tailed test.

We compute this one-tailed p-value through scipy's `ttest_ind`, which turned out to be 7.328%. This is insufficient to reject the null hypothesis if our significance level is 5%. This demonstrates that we would require more evidence to show a difference between the amount of optimal compartments in EPTs and non-EPTs.

[3]This error has been reported to Professor Melbourne. Fixing has attempted by redownloading and unzipping the `.gz` file again, but in vain.

3.2. Difference between 1 and 2 Compartment AIC

We notice that either the one-compartment or two-compartment model that had the best fit on the data. This prompts another test: what is the average ratio between the one-compartment model AIC and two-compartment model AIC.

This is an interesting statistic to know as we can know whether the improvement from one to two compartments is significantly different. For example, if the AIC for the two-compartment model is 1% higher than the one compartment model in non-EPTs, this suggests that the performance of the two are similar. Assume that with EPTs, the two-compartment model's AIC is 5% higher than one compartment model. It could suggest that it could be better to use a two-compartment model in modelling non-EPTs than EPTs as the difference between the AIC of one and two compartments is insignificant.

However, what we discover is that on average EPTs' ratio between one and two compartment model AIC is 1.0511 whereas non-EPT's ratio is 1.0509. The T-test p-value is 0.4995, suggesting that the difference between EPT's and non-EPT's ratio of AIC is insignificant. This demonstrates that the improvement for EPTs and non-EPTs from one to two compartments is insignificant, that is, if we use two-compartment models to model non-EPTs, we should do the same for EPTs too.

3.3. Difference between Optimal Model AIC

We compare the difference between each patient's optimal model's AIC to see how well on average the best model is between the EPTs and non-EPTs. On average, EPT's best model's AIC is 89.037 and non-EPT's best model's AIC is 85.851. Upon completing a one-tailed T-test, it gave a p-value of 4.087%, significant enough to suggest that non-EPT's best model's AIC is better than EPTs. The analysis of this result will be placed in section 4.1.

3.4. Difference between n-Compartment AIC

We also compare the difference between the same model's AIC for EPTs and non-EPTs. The results of this suggests whether higher amount of compartments fits better for EPTs. We present the averages of the AICs and their p-value against the compartment in Table 4.

We can see that for 1 to 3 compartment models, the AIC for non-EPTs are lower than EPTs with a p-value that suggests that non-EPTs have a smaller AIC. For the 2 and 3 compartment models, it is significant to say that EPTs would be better in using those models in modelling their brain as opposed to non-EPTs. However, this improvement diminishes when we use a 4-compartment model, where both EPTs and non-EPTs have a very similar AIC. This can be suggested by their T-test p-value as well.

Model	EPT AIC	non-EPT AIC	p-value
1	89.17	86.20	5.31%
2	93.70	90.34	4.23%
3	99.40	95.56	2.91%
4	104.43	103.32	27.01%

Table 4: EPT vs non-EPT AICs on same model

Compartments	Occurrence	%age
1	442	79.211%
2	96	17.204%
3	16	2.867%
4	4	0.717%

Table 5: Compartments in the Optimally Fitted Model for one EPT patient

3.5. Voxel-wise Best Compartment Model

Since our research question is whether if a patient is EPT will lead to a decreased amount of compartments needed to optimally model their brain, we provide an insight to this question by creating a map of the amount of compartments in the optimally fitted model on one slice of the MRI.

Figure A.11 and Figure A.10 are created with the same algorithm as Figure A.7, which has been described in section 2. They describe the amount of compartments that best model has for each voxel in that slice in an EPT and an non-EPT patient respectively.

The amount of compartments in the optimally fitted model against its percentage occurrence for EPTs and non-EPTs are illustrated in Table 5 and Table 6 respectively. The expected amount of voxels for EPTs is 1.24641 and non-EPTs 1.2509. This is obtained by a weighted sum on compartments and %age in the tables.

Compartments	Occurrence	%age
1	619	80.704%
2	115	14.993%
3	25	3.259%
4	8	1.043%

Table 6: Compartments in the Optimally Fitted Model for one non-EPT patient

4. Discussion

We provide discussions onto our interpretations of the results as well as limitations to our approaches in this section. In particular, we focus on the code which checks the best amount of compartments to fit voxel-by-voxel as stated in section 2.2 in the limitations of our approach.

4.1. Analysis

In this experiment, we attempted to show that non-EPTs in general, would require a higher amount of compartments to fit their brains than EPTs. This is probably due to the fact that EPTs have a lesser amount of myelin in their brain, where myelin is particularly populated within the white matter regions of their brain.

However, we did not gather significant evidence in section 3.1 through the use of the student's T test as the p-value was not high enough. Yet, the p-value of 7.328% is still low, demonstrating that this study should still be continued considering that we fitted a simpler version of the problem which had a low SNR. This can be continued by performing a voxel-by-voxel fitting on all white matter voxels in all patients involved in this study.

We did another analysis in section 3.5, where we took two slices on the same z-axis slice on one EPT and one non-EPT from the EPICure Dataset to obtain Figure A.11 and Figure A.10 respectively. Each voxel in the two figures indicate the best amount of compartments to model that voxel's signal intensity against echo time. We can see that the expected amount of compartments needed to optimally model an EPT is higher than an non-EPT patient, for that the particular pair of patients and slice. Whether this is the general case would need to be further analysed.

Furthermore, we have provided evidence which suggest that a 2 and 3-compartment model would fit better in a non-EPT than an EPT through a student's T test on their individual AIC in section 3.4. This also suggests that potentially EPTs would require more compartments to model, which is in line with what we hypothesised. However, it might be harder to model EPT's brains as opposed to non-EPT's brains as the AIC for EPT's brains are consistently higher than non-EPTs.

It can also be seen in section 3.2 that the average increase of AIC from one to two compartment models is approximately the same in EPTs and non-EPTs, demonstrating that if we were to decide to increase the amount of compartments to model EPTs, we should do the same too for non-EPTs to avoid bias.

4.2. Implications

Although we attempted to show that the amount of compartments needed to model EPTs is lesser than non-EPTs, we did not reach a 5% significance level. Even so, in terms of the raw value, we can see that non-EPTs' number of optimal compartments is larger than EPT's.

Since we were unable to complete an extensive study due to computational constraints, we provide implications and some further works for this study if our hypothesis, i.e. 'lesser compartments are needed to model EPT's brains', is proven true in the extensive search.

If our hypothesis comes true, it suggests that EPT's myelins in the white matter regions are more sparsely located than non-EPTs therefore the white matter is less complex. This follows because compartment models are used to capture each tissue type within the voxel; therefore, as the only difference we know of between non-EPTs and EPTs is density of myelin, it follows that lesser compartments implies lesser myelin.

However, caution should also be taken; we should compare the second smallest AIC and see whether the difference between the second smallest and the smallest AIC is significant enough. For example, if the 1-compartment model had the AIC of 90 and 2-compartment model had the AIC of 91, this would not be significant enough to conclude the 1-compartment model is the best given that the absolute difference between the AICs of the 1-compartment and 2-compartment model is insignificant.

We could further this study by seeing the correlation between the average compartments and the FSIQ. If the implication that lesser compartments implies lesser myelin is true, we would expect that the IQ and average amount of compartments should also form a positive correlation. This is because myelins are known to be responsible for cognition, learning, skill development and memory [2]. This correlation can be measured using the Spearman's Correlation Coefficient or the Pearson's Correlation Coefficient.

4.3. Limitations & Future Works

A main limitation to our experiments is that we did not compute the amount of compartments that would best approximate the relationship between signal intensity and echo times voxel-by-voxel due to computation limitations.

We are unable to run the code which permutes the starting x sufficiently for all white matter voxels within every single patient. However, as a promising future works, we have constructed the code which conducts this study which leverages multi-threaded operations to increase the execution speed of this code. It is reminded to not increase

the number of max-workers in `epicure-runscript.py` file to be over the amount of CPU threads in the computer.

During the experiments, we used an Intel i7-11700F CPU to execute the code, which took 0.7 seconds if we were to permute the starting x for 10 times for 1 to 4 compartment models. We will estimate a lower bound of time needed to execute the code using that this CPU had 16-threads.

There are a total of 3,129,575 white matter voxels within all patients. Note that the code ignores non-white matter voxel, where checking if a voxel is in the white matter region consumes time. However, since we are computing a lower bound we can ignore this. Assuming that the code is to be ran on the same computer that we used for the experiments, it will take a lower bound of $3,129,575 \times 0.7 \div 16$ seconds to run, which rounds to approximately 1.58 days. This is on an assumption that there are no background tasks.

The code produces a text file, where for each patient ID, a list of AICs is paired with each AIC corresponding to each compartment model. The length of the list is the same as the amount of white matter voxels in the patient. This text file can be used for future analysis.

In our study, we also believe one weakness comes from the EPICure dataset, where we have only 10 echo times, which is not a lot to fit a 2-compartment model, 4 free-parameters model. This belief originates from the fact that the graph is already quite easy to model since it is an exponential decay. We argue that model with minimum AIC should be the 2-compartment model if there were to be more echo times. This has been shown through the use of the HD Dataset in Figure A.7.

We also conjecture that the use of the Rician Loss function to model the relationship between signal intensity and echo time could have been a better measurement since we argued that MRI noise follows a Rician Distribution. However since we do not know the noise variable σ in the expression, this limits our use of the Rician Distribution.

All in all, we provided some evidence that the amount of compartments could be correlated to whether the subject is an EPT. This has been done with several T-tests. Whether this is solidly the case would require further investigation using the code that we provided as the `epicure-runscript.py` and analysing the results that this code generated.

Code

The code has been attached with the submission and is also available in https://github.com/RcwYuen/cmbi-t2-relaxometry.

References

[1] N. Marlow, D. Wolke, M. A. Bracewell, and M. Samara, "Neurologic and developmental disability at six years of age after extremely preterm birth," *New England Journal of Medicine*, vol. 352, p. 9–19, Jan 2005.

[2] R. D. Fields, "White matter in learning, cognition and psychiatric disorders," *Trends in Neurosciences*, vol. 31, p. 361–370, Jul 2008.

[3] T. Moore, E. M. Hennessy, J. Myles, S. J. Johnson, E. S. Draper, K. L. Costeloe, and N. Marlow, "Neurological and developmental outcome in extremely preterm children born in england in 1995 and 2006: The epicure studies," *BMJ*, vol. 345, Dec 2012.

[4] B. Laureano, H. Irzan, H. O'Reilly, S. Ourselin, N. Marlow, and A. Melbourne, "Myelination of preterm brain networks at adolescence," *Magnetic Resonance Imaging*, vol. 105, p. 114–124, Jan 2024.

[5] D. Bell and J. Jones, "Mri," *Radiopaedia.org*, Jun 2009.

[6] T. Foster and J. Ballinger, "Relaxometry," *Radiopaedia.org*, Nov 2013.

[7] C. S. Parker, A. Schroder, S. C. Epstein, J. Cole, D. C. Alexander, and H. Zhang, "Rician likelihood loss for quantitative mri using self-supervised deep learning," 2023.

[8] G. S. Ioannidis, K. Nikiforaki, G. Kalaitzakis, A. Karantanas, K. Marias, and T. G. Maris, "Inverse laplace transform and multiexponential fitting analysis of t2 relaxometry data: A phantom study with aqueous and fat containing samples," *European Radiology Experimental*, vol. 4, May 2020.

[9] M. J. Cardoso, M. Modat, R. Wolz, A. Melbourne, D. Cash, D. Rueckert, and S. Ourselin, "Geodesic information flows: Spatially-variant graphs and their application to segmentation and fusion," *IEEE Transactions on Medical Imaging*, vol. 34, p. 1976–1988, Sep 2015.

Appendix A. Figures

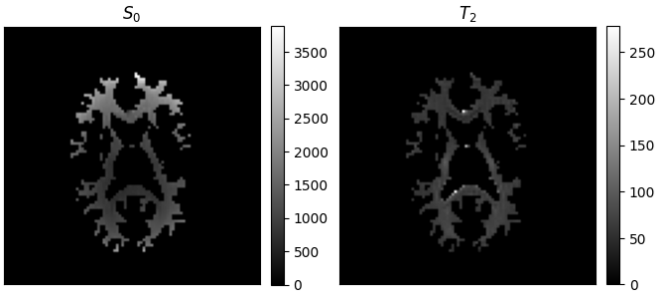

Figure A.1: Estimation of S_0 and T_2 from Normal Equation

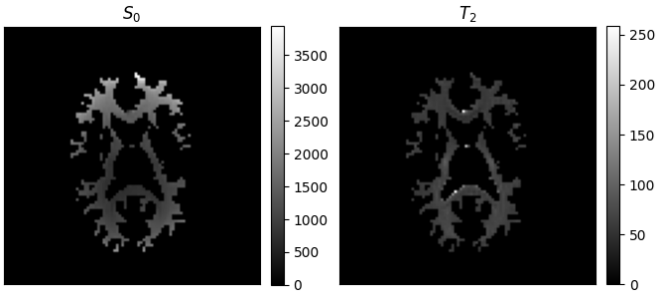

Figure A.2: Estimation of S_0 and T_2 of White Matter from Gradient Descent

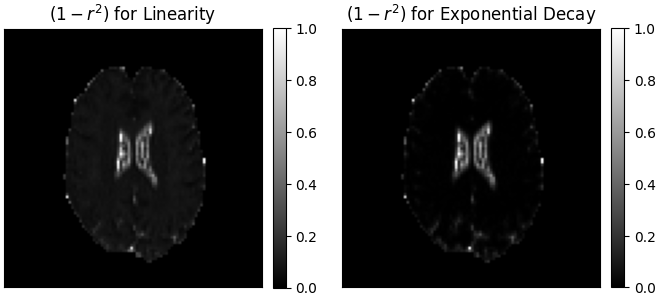

Figure A.3: Inverted r^2 Map for Centre Slice in Axial View

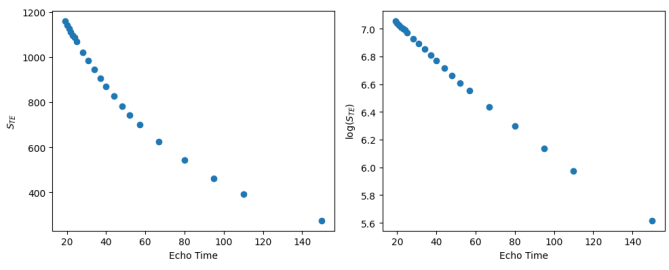

Figure A.4: r^2 for linear decrease and exponential decay on one voxel

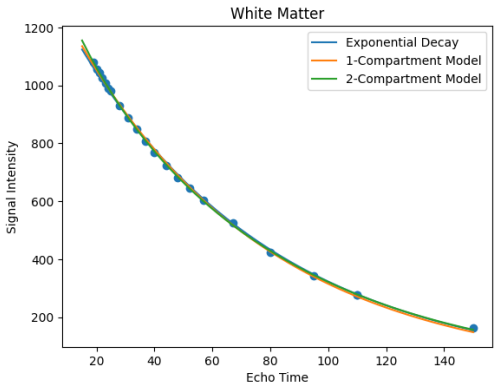

Figure A.5: Fitting of Exponential Decay

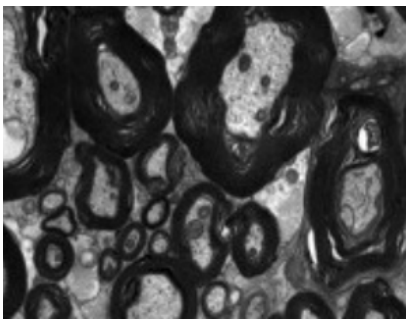

Figure A.6: White Matter under the Electro-Microscope

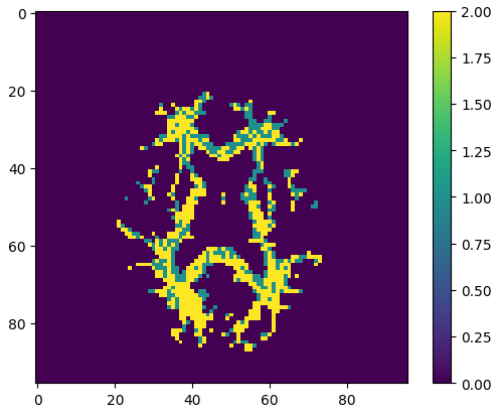

Figure A.7: Map of Minimum AIC on Sample No. 4, Axial View Slice No. 27

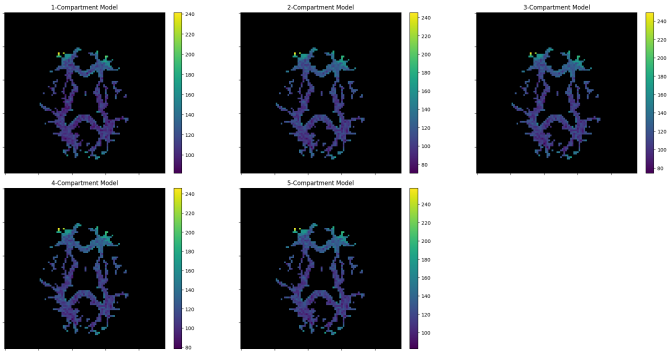

Figure A.8: Map of AIC for Sample No. 4 for each model, Axial View Slice No. 27

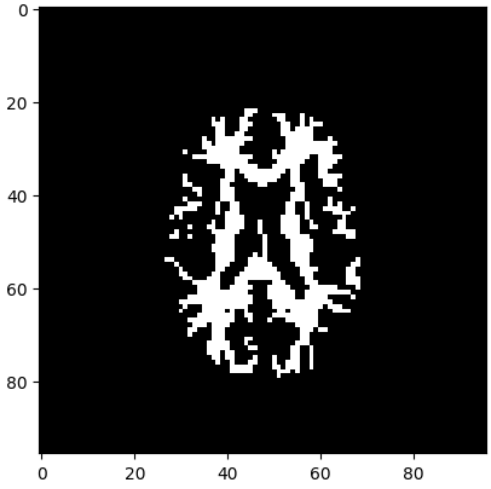

Figure A.9: Sample White Matter Segmentation mask

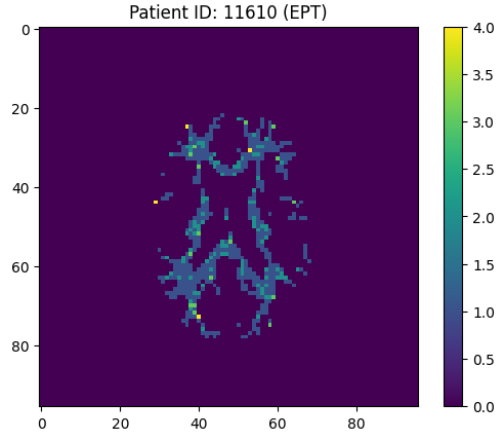

Figure A.11: EPT voxel-wise best compartment model

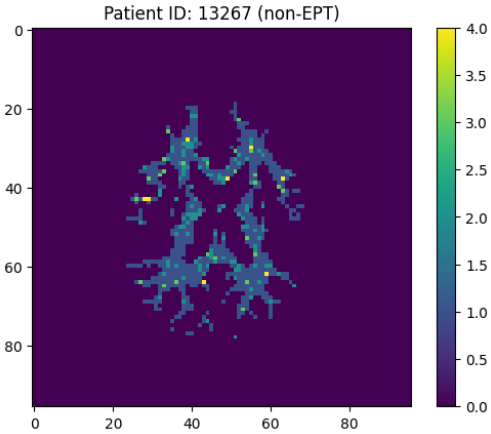

Figure A.10: Non-EPT voxel-wise best compartment model